Development of High-Sensitivity Piezoresistive Pressure Sensors for -0.5...+0.5 kPa

Mikhail Basov (engineerbasovm@gmail.com)
Dukhov Automatics Research Institute (VNIIA) https://orcid.org/0000-0003-0798-4500
Denis Prigodskiy
Dukhov Automatics Research Institute (VNIIA)

Research Article

Keywords: piezoresistive pressure sensors, high-sensitivity, modeling, nonlinearity, stops

Posted Date: July 29th, 2021

DOI: https://doi.org/10.21203/rs.3.rs-658943/v1

Development of High-Sensitivity Piezoresistive Pressure Sensors for -0.5…+0.5 kPa

Mikhail Basov, Denis Prigodskiy

Dukhov Automatics Research Institute (VNIIA), Moscow, Russian Federation

E-mail: engineerbasovm@gmail.com

Received xxxxxx
Accepted for publication xxxxxx
Published xxxxxx

Abstract

A mathematical model of an ultrahigh sensitivity piezoresistive chip of a pressure sensor with a range from -0.5 to 0.5 kPa has been developed. The optimum geometrical dimensions of a specific silicon membrane with a combination of rigid islands to ensure a trade-off relationship between sensitivity ($S_{samples}$ = 34.5 mV/kPa/V) and nonlinearity ($2K_{NL}$ samples = 0.81 %FS) have been determined. The paper also studies the range of the membrane deflection and makes recommendations on position of stops limiting diaphragm deflection in both directions; the stops allow for increasing burst pressure P_{burst} up to 450 кPa. The simulated data has been related to that of experimental samples and their comparative analysis showed the relevance of the mathematical model (estimated sensitivity and nonlinearity errors calculated on the basis of average values are 1.5% and 19%, respectively).

Keywords: piezoresistive pressure sensors, high-sensitivity, modeling, nonlinearity, stops

1. Introduction

There has been constant development of piezoresistive pressure sensor chips with ultrahigh sensitivity, which offers new approaches to the solution of the following relevant tasks:

- Enhancement of sensitivity;
- Reduction in size;
- Decrease of errors of:
  - nonlinearity,
  - temperature dependencies,
  - time stability;
- Increase of overload ability.

The knowledge of the relationship between the above parameters facilitates the development and adaptation of OEM elements in medical applications (CPAP and spirometry), ventilation systems (VAV and HVAC), automotive (TPMS and exhaust gas circulation), custom appliances (drones and smart devices) and other industries (e.g., power and aerospace industries) [1-3]. The market segment of silicon piezoresistive pressure sensors is sufficiently large and is progressively developing [4-9] and the reason for this trend is the need for fabrication of this new chip. The main objective is to create a pressure sensor operating in a differential pressure range of -0.5 to +0.5 кPa with sensitivity S > 30.0 mV/кPa/V, a nonlinearity error $2K_{NL}$ < 1.5 %FS and mechanical overload ability P_{burst} > 300 кPa. The design presented in the paper is based on the simulation of operation of the selected membrane structure. The model of an ultrahigh sensitivity chip is eventually analyzed with regard to the experimental data from the obtained samples.

2. Methods

2.1 Pressure sensor design

A classical Wheatstone resistive bridge is used as an electric circuit for the topside of a pressure sensor chip. The

most important starting condition for the design of a pressure sensor chip is its area, 6.15x6.15 mm in this case (Figure 1). Frame area on the backside of the sensor chip is used for a fluid-proof connection with a bottom stop – an intermediate element of silicon assembly (frame width Y = 690 μm). Bottom stop provides isolation of the sensor chip from thermomechanical packaging stress and enhances mechanical strength of the silicon assembly. A diaphragm with rigid islands (RI's) is formed in the central part of the sensor chip with help of anisotropic wet etching. Side walls of the etched cavity form angle of 54.7° with the plane of the wafer (width of side wall projection on the plane of the wafer is G = 285 μm). The final area for a thinned part of the membrane is 4.20x4.20 mm. The other essential factor is the design strength. Based on the data of similar available analogs, e.g. from SMi (SM95G) and Acuity (AC3070) [10,11], or presented in the articles [12,13], it can be said even without building a mathematical model that the chip should be connected with the stops to achieve the burst pressure that 600 times as large as the rated pressure.

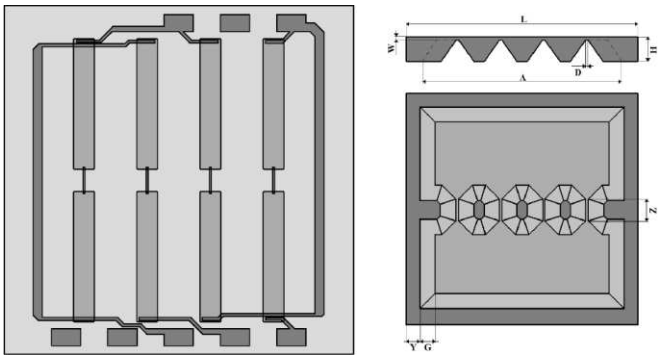

Fig. 1. Schematic representation of an ultrahigh sensitivity pressure sensor chip.

The mechanical part of pressure sensor includes a membrane structure with three separate mechanical stress (MS) concentrators or rigid islands (RI), and two MS concentrators connected to the frame. The thickness of RIs is equal to the wafer thickness. The selected structure of the membrane with RIs allows concentrating high MS at small deflections, which reduces a nonlinearity error [14, 15]. The geometrical parameters of the chip are as follows: L – chip side length, W – thickness of the membrane thinned part, H – chip thickness, A – area of the membrane thinned part, D – width of a gap between RIs, Z – RI edge length, Y – chip frame width, G – membrane etch taper projection width. Pairs of piezoresistors (PRs) with a dimension of 20x400 μm are located on the thinned part of the membrane in the regions of compression and tension, i.e. of MS of different signs. Although reactive ion etching (RIE) of silicon is widely employed for fabrication of chips for ultra-low pressure ranges [16-21], the membrane structure is formed using wet anisotropic etching without use of RIE from either the top or back side of the chip**.**

It is worth noting that alternative electric circuits may be used for similar ultrahigh sensitivity chips either to enhance the sensitivity or decrease the dimensions of a chip relative to its analogs with a resistive bridge by combining together a large number of PRs. The novel electric circuit is made as the differential amplifier (PDA) using BJT [22-25]. The development of such pressure sensor chips is still at the beginning of the road, but the mathematical model and experimental data, that have already been demonstrated, indicate that PDA has an obvious advantage in this application.

2.2 Modelling of Sensitivity and Nonlinearity

The structure of a pressure sensor chip was modeled and experimentally fabricated on silicon wafers n-type with a crystal orientation (100). PRs, used in a classical Wheatstone resistive bridge, are oriented along the crystallographic direction [110] and formed, using boron doping (p^--region), with the following parameters: surface concentration $N_{Sp-} = 5.5 \cdot 10^{18}$ cm^{-3}, surface resistance $R_{Sp-} = 200$ Ohm/cm^{-2}, depth of a p-n junction $x_{jp-} = 2.5$ μm. The main piezoresistive coefficient $\pi_{44} = 1.26 \cdot 10^{-9} \cdot$Pa^{-1} at room temperature [26]. In order to connect PRs with metal layer, high-alloy conducting p^+ regions ($N_{sp+} = 7.4 \cdot 10^{19}$ cm^{-3}, $x_{jp+} = 3.6$ μm, $R_{sp+} = 17$ Ohm/cm^{-2}) are also used, they have a sufficiently low piezoresistive coefficient and are located in regions of low stresses. A contribution of p^+ conducting regions in a computing model is not significant and will be not taken into consideration. A thin aluminum layer ($W_{Al} = 0.8$ μm), applied on the chip frame [27-30], is needed to reduce temperature hysteresis.

The calculation of a change in the PR value and, consequently, output sensitivity and nonlinearity is carried out based on the theory of piezoresistive effect from the following formulas:

$$\Delta R_i = \frac{1}{2} \cdot \pi_{44} \cdot \sigma(\Delta P) \cdot R_i, \quad (1)$$

$$\Delta V_{out}(\Delta P) = \frac{(R_1 + \Delta R_1(\Delta P)) \cdot (R_3 + \Delta R_3(\Delta P)) - (R_2 + \Delta R_2(\Delta P)) \cdot (R_4 + \Delta R_4(\Delta P))}{(R_1 + \Delta R_1(\Delta P) + R_2 + \Delta R_2(\Delta P)) \cdot (R_3 + \Delta R_3(\Delta P) + R_4 + \Delta R_4(\Delta P))} \cdot V_{in}, \quad (2)$$

$$S = \frac{\Delta V_{out}(\Delta P)}{V_{in} \cdot \Delta P}, \quad (3)$$

$$2K_{NL\,j}(\Delta P) = \frac{\Delta V_{out}(\Delta P) - \frac{\Delta V_{out}(0.5kPa) - V_0}{0.5kPa} \cdot \Delta P}{\Delta V_{out}(0.5kPa)}, \quad (4)$$

Equation where R_i – PR value (i = 1, 2, 3, 4); $\Delta R_i(\Delta P)$ – change of PR value (i = 1, 2, 3, 4) at applied pressure ΔP; ΔP – applied pressure value; π_{44} – piezoresistive coefficient for p-type impurity, plane (100) and direction [110]; $\sigma(\Delta P)$ – MS value at applied pressure ΔP; $\Delta V_{out}(\Delta P)$ – bridge circuit output signal at applied pressure ΔP; V_{in} – bridge circuit supply voltage (5 V); S – sensitivity; $2K_{NL}$ – output signal

nonlinearity error; V_0 – output signal at ΔP = 0.0 κPa; ΔV_{out}(0.5 kPa) – output signal at ΔP = 0.5 κPa.

With the selected membrane structure, variation of different geometrical parameters was considered: (a) RI width (Figure 2; Q1 – distance between middle PRs, Q2 – distance between end PRs), (b) RI edge length, (c) gap between RIs, and (d) the membrane thickness. In order not to overburden the paper with statistical data, we will present only the most relevant options of variation of one of the parameters, provided the selected optimum values for the rest of geometrical dimensions of the membrane remain unchanged. The sensitivity and nonlinearity are calculated using average MS values across ZxD areas in equations (1-4). The pressure is applied from the backside of the chip in a range of 0.0 to 0.5 κPa and an increment of 0.1 κPa. When assessing sensitivity and, which is more important, nonlinearity, it is necessary to take into consideration a possible spread in the parameters to ensure that the final samples satisfy the requirements for the parameters at the bottom boundary of the array. Therefore, it is desirable to achieve S > 35.0 mV/κPa/V and $2K_{NL}$ < 0.75 %FS.

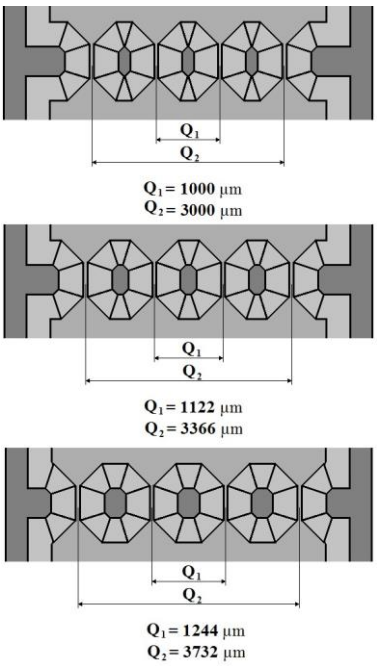

Fig. 2. Options of variation of RI width and, consequently, PR location on the membrane.

Figure 2 presents options of PR layout when the width of RIs varies and the area of the thinned part A of the membrane remains unchanged. The optimum geometry at variation of the RI width is a ratio Q_1/Q_2 = 1122/3366 µm as the balance between sensitivity and nonlinearity is maintained (Figure 3(a)). At Q_1/Q_2 = 1000/3000 µm sensitivity is S < 20 mV/κPa/V and at Q_1/Q_2 = 1244/3732 µm nonlinearity is relatively high at a lower sensitivity (relative to Q_1/Q_2 = 1122/3366 µm). At variation of the length of a RI edge one more significant feature associated with a spread in the values of the RI edge length should be taken into consideration. As seen from Figure 3(b), Z = 400 µm is the optimum value as at a smaller value of Z = 300 µm there is an acceptable enhancement of both sensitivity and nonlinearity, further decreasing will result in a considerable growth of nonlinearity. In the opposite situation at Z = 500 µm sensitivity and nonlinearity sufficiently decrease, further increasing will result in lower sensitivity. The estimate of the output parameters relative to a change in the width of a gap between RIs (Figure 3(c)) shows that the optimum rated width of a gap is 10 µm. But we have again to deal with the spread that makes it problematic to guarantee a required width of a gap of 10 µm with the largest possible thinning-down of the membrane for PR of width 20µm at photolithography (24.2 µm with regard to a contribution of sideways diffusion). The width of a gap should be preferably increased up to D = 18 µm even at the expense of a small reduction of sensitivity. As expected, the sensitivity and nonlinearity sharply change with a change of the membrane thickness (Figure 3(d)). Theoretical computation showed that the membrane thickness should be W = 8 µm and a spread in the thickness should be minimum as its increase or decrease could lead to significant reduction of sensitivity or growth of nonlinearity, respectively.

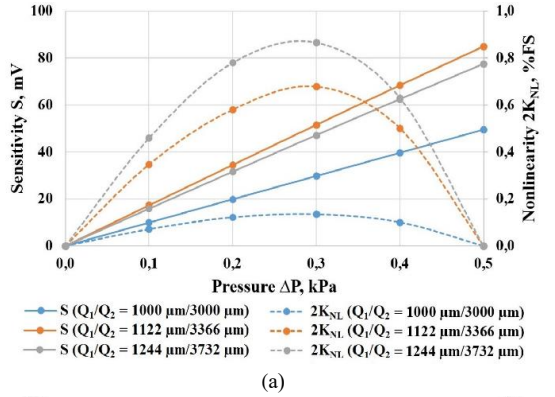

(a)

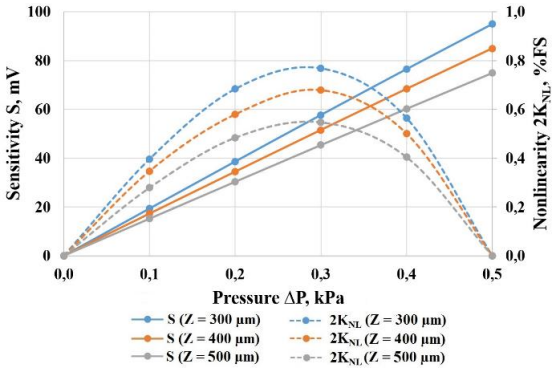

(b)

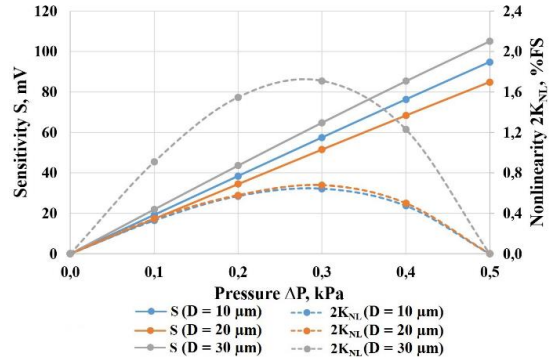

(c)

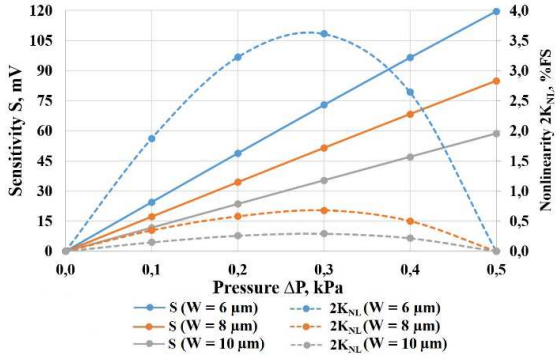

(d)

Fig. 3. Sensitivity (solid line) and nonlinearity (dot line) dependences on the pressure at variation of: (a) RI width Q_1/Q_2, (b) RI edge length Z, (c) width of a gap between RIs D, (d) membrane thickness W.

Figure 4 depicts maps of MS distribution and membrane deflection at a pressure of 0.5 κPa.

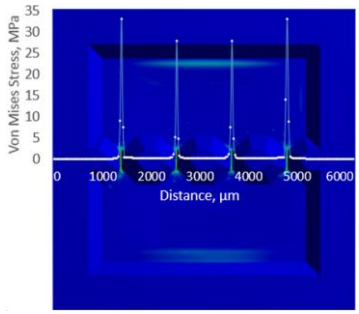

(a)

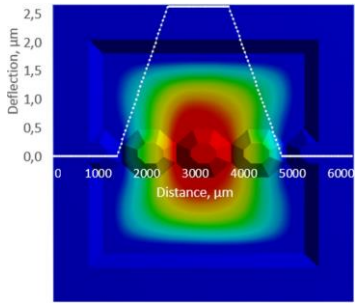

(b)

Fig. 4. Maps of MS distribution (a) and membrane deflection (b) for the membrane geometry at 0.5 κPa.

Table 1 contains final geometrical dimensions that are selected for realization of an ultrahigh sensitivity pressure sensor chip.

Table 1. Optimum geometrical dimensions of a pressure sensor chip with ultrahigh sensitivity.

Geometrical parameters of chip	L	Q_1/ Q_2	W	H	A	D	Z	Y	G
Values, μm	6150	1122/ 3366	8	420	4200	18	400	690	285

The mathematical model eventually permits to predict fabrication of samples with an average sensitivity S_{model} = 34.0 mV/κPa/V and nonlinearity $2K_{NLmodel}$ = 0.68 %FS. The membrane deflection at the rated pressure is $\Delta h_{0,5}$ = 2.7 μm.

2.3 Modelling of Increased Strength

In order to increase the strength of a chip, the silicon assembly utilizes stops from both sides of the chip (Figure 5): the bottom stop is fabricated as an intermediate element between the chip and the base, it is connected across the area of the chip frame and has via holes through which pressure is applied from the base; the top stop is made as a regular parallelepiped, it is connected from both sides of the chip in points without metallic pads and has unconnected areas to apply pressure from the topside of the chip. The elements of the assembly including a chip, top and bottom stops and a base are bonded using low temperature glass, the combination of the glass and the selected assembly allow lessening a thermo-mechanical effect from the package [31].

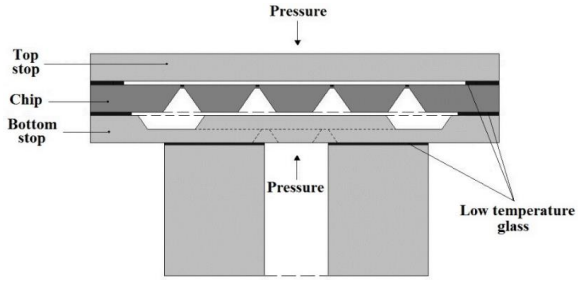

(a)

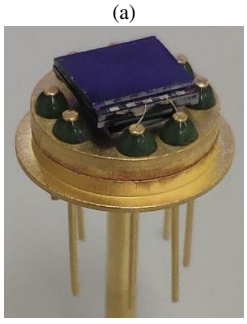

(b)

Fig. 5. Assembly design: (a) schematic connection of a chip, stops and a base; (b) a pressure sensor assembly in the package.

A gap between the chip membrane and the bottom and top stops that determines a free movement of the membrane is ensured by the thickness of low temperature glass. The movement of the membrane should be free in an operating pressure range of -0.5 to +0.5 κPa with a reasonable margin in order to exclude the possibility of early touching, which can significantly influence nonlinearity of an output signal. The movement of the membrane should be additionally held by the stops before the structure is on the point of destruction. Theoretically, irreversible critical deformable states can be achieved at $\sigma_{chip.\ theor.} < 500$ MPa [32]. Figure 6 presents the relationship between the maximum MS, deflection of the middle of the membrane and the pressure. With regard to these conditions, the membrane should be set on the stops in a pressure range $P_{touch\ model}$ of 1.0 to 4.5 κPa. The simulation of the geometry of the membrane deflection in the given pressure range permits to conclude that the thickness of the low temperature glass is great enough to guarantee a gap between the chip and the stop $h_{touch\ model}$ of 5 to 23 μm needed to provide the required membrane deflection.

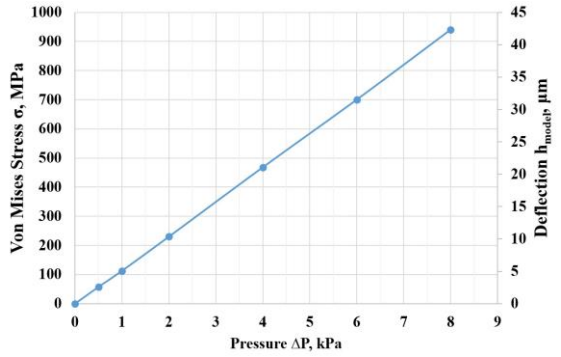

Fig. 6. Simulated dependence of end PR MS and the membrane middle deflection on the pressure (up to 8 κPa) for an ultrahigh sensitivity pressure sensor.

3. Results

Based on the built mathematical model, samples of ultrahigh sensitivity chip of pressure sensors were obtained. The results of the implementation of technological processes aimed to form the topside of the chip guaranteed a spread in surface resistance R_S (surface impurity concentration N_S) and, consequently, resistor value (R_{bridge} = 4.5 κOhm) within 7% error (output signal $\Delta V_{0samples}$ = -5…+5 mV/V At anisotropic wet etching without self-hardening a spread in the membrane thickness was ΔW = ± 3 μm on 5 plates 100 mm in diameter. For further investigation chips with a thickness W_{sample} of 8 to 9 μm were selected in order to get as far as possible closer to the values of the chip geometry in the mathematical model. Besides a spread in the membrane thickness, there is also an asymmetry in the layout of RI edges on the samples (Figure 7).

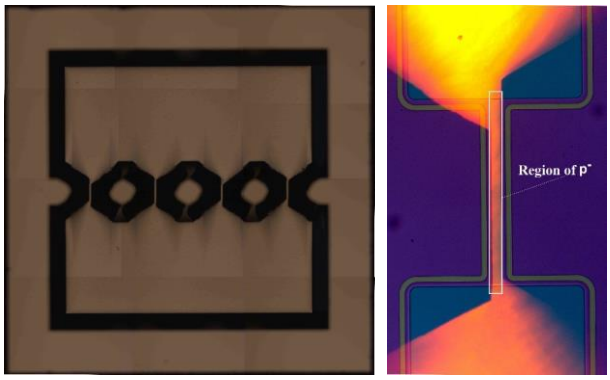

(a) (b)

Fig. 7. Membrane of experimental samples: (a) general view; (b) layout of PR p^--regions relative to RI structure.

Table 2 contains the values and errors of input parameters (the membrane geometry) and output electric parameters of 62 obtained samples.

Table 2. Input and output parameters of an ultrahigh sensitive pressure sensor chip.

Parameters	Designation	Value	Dimension
Input			
Membrane thickness	$W_{samples}$	8…9	μm
Distance between RI	$D_{samples}$	18 ± 3	
Edge length of RI	$Z_{samples}$	400 ± 60	
Output			
Sensitivity (backside)	$S_{samples}$	34.2 ± 3.9	mV/kPa/V
Sensitivity (topside)		34.8 ± 4.2	
Nonlinearity (backside)	$2K_{NLsamples}$	0.77 ± 0.48	%FS
Nonlinearity (topside)		0.85 ± 0.52	
Zero output signal	$V_{0samples}$	-5…+5	mV/V
Numbers	-	62	samples

There is some difference in the values of sensitivity and nonlinearity when pressure is applied from the topside and the backside of the chip. The volume of chips exhibits residual MS (compressive stresses) arising from a step structure of silicon oxide SiO_2 (W_{SiO2} = 0.2…0.6 μm), obtained at formation of different types of doped regions without compensation of MS (tensile stresses) from a layer of silicon nitride Si_3N_4 [33-37]. After a theoretical value of an output signal is calculated for each individual sample as an arithmetic average of the output signal values at $\Delta V_{out}(\Delta P_+ = 0.1\ \text{κPa})_{samples}$ and $\Delta V_{out}(\Delta P_- = -0.1\ \text{κPa})_{samples}$ and compared with $V_{0samples}$, it can be concluded that the membrane is bent upwards (as shown in Figure 3(a)) with MS average of the order of σ_r = 0.15 MPa ($\Delta V_0(\sigma_r)$ = 0.26 mV).

Tests of samples for an overload ability showed that the membrane of ultrahigh sensitivity chips breaks at $P_{burst\ without\ stops} \approx 9$ κPa independently of the direction in which pressure is applied. Figure 8 gives an example of output signal variation (relative to an output signal of each sample at P = 0 κPa) for ten typical samples with stops (a

blue sector refers to the operating pressure range). As seen from the analysis of the dependencies, the membrane is set on the stops from both sides in a pressure range $P_{touch\ samples}$ of 2 to 5 кPa. The area of the surface-to-surface contact of the membrane and the stops at an additional overload pressure is gradually re-allocated and the sensor breaks down at the pressure P_{burst} above 450 кPa.

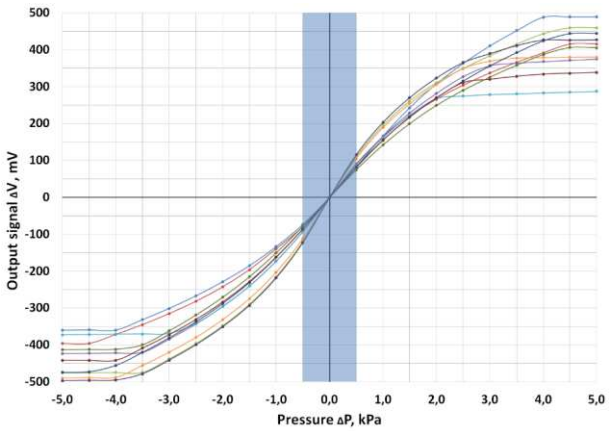

Fig. 8. Output signal dependencies on the pressure for several typical samples of an ultrahigh sensitivity pressure sensor.

4. Conclusion

In the course of the development of an ultrahigh sensitivity, pressure sensor a mathematical model for the selected design of a chip with a resistive bridge circuit has been built and used to obtain and investigate a certain amount of samples. The optimum geometry of the membrane for chips of pressure sensor, operating in a range of -0.5 to +0.5 kPa, has been defined based on a possible trade-off relationship between sensitivity and nonlinearity. A comparative analysis of average values of the simulated data (S_{model} = 34.0 mV/кPa/V and $2K_{NLmodel}$= 0.68 %FS) and experimental data ($S_{samples}$ = 34.5 mV/кPa/V and $2K_{NLsamples}$ = 0.81 %FS) showed that the model was capable of predicting operating modes of the selected chip design on the basis of average values with sensitivity and nonlinearity errors of 1.5% and 19%, respectively. A considerable difference between nonlinearity errors of the calculated and experimental values is due to a SiO_2 layer on the samples; at the early stages of the model development SiO_2 was not taken into account. It is necessary to narrow a spread in the output characteristics of sensors through technological upgrading [38-46] for making a more detailed assessment of the model and increase the percentage of samples with desired parameters. The technological upgrading includes dry and wet stop-etching, compensation of residual MS on chips from SiO_2 and Si_3N_4 films, precision alignment at lithography relative to an orientation flat of the wafer or use of silicon wafers with initial low misorientation of the crystal orientation and orientation flat [47,48].

A silicon assembly with top and bottom stops to increase burst pressure of a sensor has been additionally developed. Based on the mathematical model, a technological process for bonding chips with stops has been implemented, which makes it possible to achieve the required gap for a free movement of the membrane in the operating range up to the moment of breaks ($P_{touch\ samples}$ = 2…5 kPa). The sensor breaks at P_{burst} above 450 кPa, which satisfies the required conditions with X1,5 margin.

Acknowledgements

The studies were financially supported by Dukhov All-Russia Research Institute of Automatics.

References

[1] https://www.i-micronews.com/products/mems-pressure-sensor-market-and-technologies-2018

[2] https://www.i-micronews.com/smi-launches-mems-ultra-low-pressure-sensor

[3] https://www.i-micronews.com/products/melexis-mlx91802-absolute-pressure-sensor

[4] L. Li, N. Belov, M. Klitzke, J-S. Park, High Performance Piezoresistive Low Pressure Sensors, IEEE Sensors Conference (2016) 1406-1408.

[5] X. Huang, D. Zhang, A High Sensitivity and High Linearity Pressure Sensor Based on a Peninsulastructured Diaphragm for Low-Pressure Ranges, Sensors and Actuators A: Physical 216 (2014) 176-189.

[6] S. Marco, J. Samitier, O. Ruiz, J.R. Morante, J. Esteved, High-Performance Piezoresistive Pressure Sensors for Biomedical Applications Using Very Thin Structured Membranes, IOP Measurement Science and Technology 7 (1996) 1195-1203.

[7] Yu, Z., Zhao, Y., Sun, L., Tian, B., Jiang, Z., 2013. Incorporation of Beams into Bossed Diaphragm for a High Sensitivity and Overload Micro Pressure Sensor. Review Scientific Instruments. 84, 015004.

[8] A. Berns, U. Buder, E. Obermeier, A. Wolter, A. Leder, AeroMEMS sensor array for high-resolution wall pressure measurements, Sensors and Actuators A: Physical 132 (2006) 104-111.

[9] K.C. Katuri, S. Asrani, M.K. Ramasubramanian, Intraocular Pressure Monitoring Sensors, IEEE Sensors Journal 8 (2008) 12–19.

[10] https://www.si-micro.com/products/mems-die/ultra-low-pressure-sm95g.html

[11] http://www.acuitymicro.com/Products.htm#Pressure Die

[12] X. Huang, D. Zhang, Structured diaphragm with a centre boss and four peninsulas for high sensitivity and high linearity pressure sensors, Micro and Nano Letters 9 (2014) 460-463.

[13] Zhao, L., Xu, T., Hebibul, R., Jiang, Z., Ding, J., Peng, N., Guo, X., Xu, Y., Wang, H., Zhao, Y., 2016. A

Bossed Diaphragm Piezoresistive Pressure Sensor with a Peninsula-Island Structure for the Ultra-Low-Pressure Range with High Sensitivity. IOP Measurement Science and Technology. 27, 124012.

[14] S. Timoshenko, S. Woinowsky-Krieger, Theory of Plates and Shells, MCGraw-Hill, New York, 1970.

[15] N.S. Zemlyannikov, N.L. Danilova, V.V. Pankov, V.S. Sukhanov, Yu.A. Mikhailov, Tensoresistive Pressure Sensors on the Basis of Complex-Profled Silicon Membranes, Nano- and Microsystem Technology 4 (2013) 32-35.

[16] Tran, A.V., Zhang, X., Zhu, B., 2018. Mechanical Structural Design of a Piezoresistive Pressure Sensor for Low-Pressure Measurement: A Computational Analysis by Increases in the Sensor Sensitivity. Sensors. 18, 2023.

[17] Xu, T., Lu, D., Zhao, L., Jiang, Z., Wang., H., Guo, X., Li, Z., Zhou, X., Zhao, Y., 2017. Application and Optimization of Stiffness Abruption Structures for Pressure Sensors with High Sensitivity and Anti-Overload Ability. Sensors. 17, 1965.

[18] N. Arjunan, S. Thangavelu, Modeling and Analysis of a Multi Bossed Beam Membrane Sensor for Environmental Applications, Transactions on Electrical and Electronic Materials 18 (2017) 25–29.

[19] R.H. Johnson, S. Karbassi, U. Sridhar, B. Speldrich, A High-Sensitivity Ribbed and Bossed Pressure Transducer, Sensors and Actuators A: Physical 35 (1992) 93-99.

[20] A. Wu, J. Chen, X. Wang, A very sensitive pressure sensor on a SOI on cavity substrate, Proceedings of IEEE International SOI Conference (2007) 151–152

[21] C.T. Seo, Y.M. Kim, J.K. Shin, J.H. Lee, A Novel Comb-Type Differential Pressure Sensor with Silicon Beams Embedded in a Silicone Rubber Membrane, Jpn. J. Appl. Phys. 43 (2004) 2046–2049.

[22] M.V. Basov, D.M. Prigodskiy, Investigation of a Sensitive Element for the Pressure Sensor Based on a Bipolar Piezotransistor, Nano- and Microsystem Technology 19 (2017) 685-693.

[23] M.V. Basov, D.M. Prigodskiy, D.A. Holodkov, Modeling of Sensitive Element for Pressure Sensor Based on Bipolar Piezotransistor, Sensors and Systems 6 (2017) 17-24.

[24] M. Basov, Development of High-Sensitivity Pressure Sensor with On-chip Differential Transistor Amplifier, Journal of Micromechanics and Microengineering, 30 (2020) 065001.

[25] M. Basov, High-sensitivity MEMS pressure sensor utilizing bipolar junction transistor with temperature compensation, Sensors and Actuators A: Physical, 303 (2020) 111705.

[26] Y. Kanda, A Graphical Representation of the Piezoresistance Coefficients in Silicon, IEEE Transactions on electron devices 29 (1982) 64-70.

[27] Liu, Y., Wang, H., Zhao, W., Qin, H., Fang, X., 2016. Thermal-performance instability in piezoresistive sensors: Inducement and improvement. Sensors. 16, 1984.

[28] J.A. Chiou, S. Chen, Thermal hysteresis analysis of MEMS pressure sensors, Journal of Microelectromechanical Systems 14 (2005) 782-787.

[29] H.N. Chiang, T.L. Chou, C.T. Lin, K.N. Chiang, Investigation of the hysteresis phenomenon of a silicon-based piezoresistive pressure sensor, IEEE Conference International Microsystems, Packaging, Assembly and Circuits Technology (2007), 165-168.

[30] S. Guo, H. Eriksen, K. Childress, A. Fink, M. Hoffman, High temperature smart-cut SOI pressure sensor, Sensors and Actuators A: Physical 154 (2009) 255–260.

[31] D.M. Prigodskiy, M.V. Basov, Research of Pressure Sensitive Elements with Increased Strength, Nano- and Microsystem Technology, Nano- and Microsystem Technology 6 (2019) 368-376.

[32] X.P. Wu, A New Pressure Sensor with Innercompensation for Nonlinearity and Protection to Overpressure, Sensors and Actuators A 21 (1990) 65-69.

[33] A.V. Tran, X. Zhang, B. Zhu, Effects of temperature and residual stresses on the output characteristics of a piezoresistive pressure sensor, IEEE Access 7 (2019) 27668-27676.

[34] T. Guan, F. Yang, W. Wang, X. Huang, B. Jiang, D. Zhang, The Design and Analysis of Piezoresistive Shuriken-Structured Diaphragm Micro-Pressure Sensors, Journal of Microelectromechanical Systems PP(99) (2016) pp. 1-9.

[35] C. Iliescu, M. Avram, B. Chen, A. Popescu, V. Dumitrescu, D.P. Poenar, A. Sterian, D. Vrtacnik, S. Amon, P. Sterian, Residual stress in thin films PECVD deposition: a review, Journal of Optoelectronics and Advanced Materials 4 (2011) 387-394.

[36] Nie, M., Bao, H., 2016. A theoretical model and analysis of composite membrane of a piezoresistive pressure sensor. AIP Advances. 6, 105302.

[37] P.K. Guo, J. King, M. Lester, R. Craddock, A Hollow Stiffening Structure for Low-Pressure Sensors, Sensors and Actuators A: Physical 160 (2010) 35–41.

[38] Li, C., Cordovilla, F., Jagdheesh, R., Ocana, J.L., 2018. Design Optimization and Fabrication of a Novel Structural SOI Piezoresistive Pressure Sensor with High Accuracy. Sensors. 18, 439.

[39] P. Mackowiak, M. Schiffer, X. Xu, E. Obermeier, H. Ngo, Design and Simulation of Ultra High Sensitive Piezoresistive MEMS Sensor With Structured Membrane for Low Pressure Applications, 12th Electronics Packaging Technology Conference, (2010) 757-761.

[40] H. Sandmaier, K. Kuhl, A square-diaphragm piezoresistive pressure sensor with a rectangular central boss for low-pressure ranges, IEEE Transactions on Electron Devices 40 (1993) 1754-1759.

[41] A.A. Barlian, W.T. Park, J.R. Mallon, A.J. Rastegar, B.L. Pruitt, Review: Semiconductor piezoresistance for microsystems, Proceedings of the IEEE, 97 (2009) 513–552.

[42] M. Bao, L. Yu, Y. Wang, Micromachined beam-diaphragm structure improves performances of pressure transducer. Sensors and Actuators A: Physical 21 (1990) 137–141

[43] S. Armbruster, F. Schafer, G. Lammel, H. Artmann, C. Schelling, H. Benzel, S. Finkbeiner, F. Larmer, P. Ruther, O. Paul, A novel micromachining process for the fabrication of monocrystalline Si-membranes using porous silicon, The 12th International Conference on Solid-State Sensors, Actuators, and Microsystems (2003) 246–249.

[44] G. Lammel, S. Armbruster, C. Schelling, H. Benzel, J. Brasas, M. Illing, R. Gampp, V. Senz, F. Schafer, S. Finkbeiner, Next generation pressure sensors in surface micromachining technology, The 13th International Conference on Solid-State Sensors, Actuators, and Microsystems (2005) 35–36.

[45] B. Kloeck, S. D. Collins, N. F. de Rooij, R. L. Smith, Study of electrochemical etch-stop for high-precision thickness control of silicon membranes, IEEE Trans. Electron Devices 36 (1989) 663–669.

[46] K. Petersen, P. Barth, J. Poydock, J. Brown, J. J. Mallon, J. Bryzek, Silicon fusion bonding for pressure sensors, Tech. Digest 1988 IEEE Solid-State Sensor and Actuator Workshop (1988) 144–147.

[47] V. Lindroos, M. Tilli, A. Lehto, T. Motooka, Handbook of Silicon Based MEMS Materials and Technologies, William Andrew Applied Science Publishers, Oxford, 2010.

[48] J.C. Doll, B.L. Pruitt, Alternative Materials and Transduction Methods, in: Piezoresistor Design and Applications. Microsystems and Nanosystems, vol 1., Springer, New York, 2013.

Figures

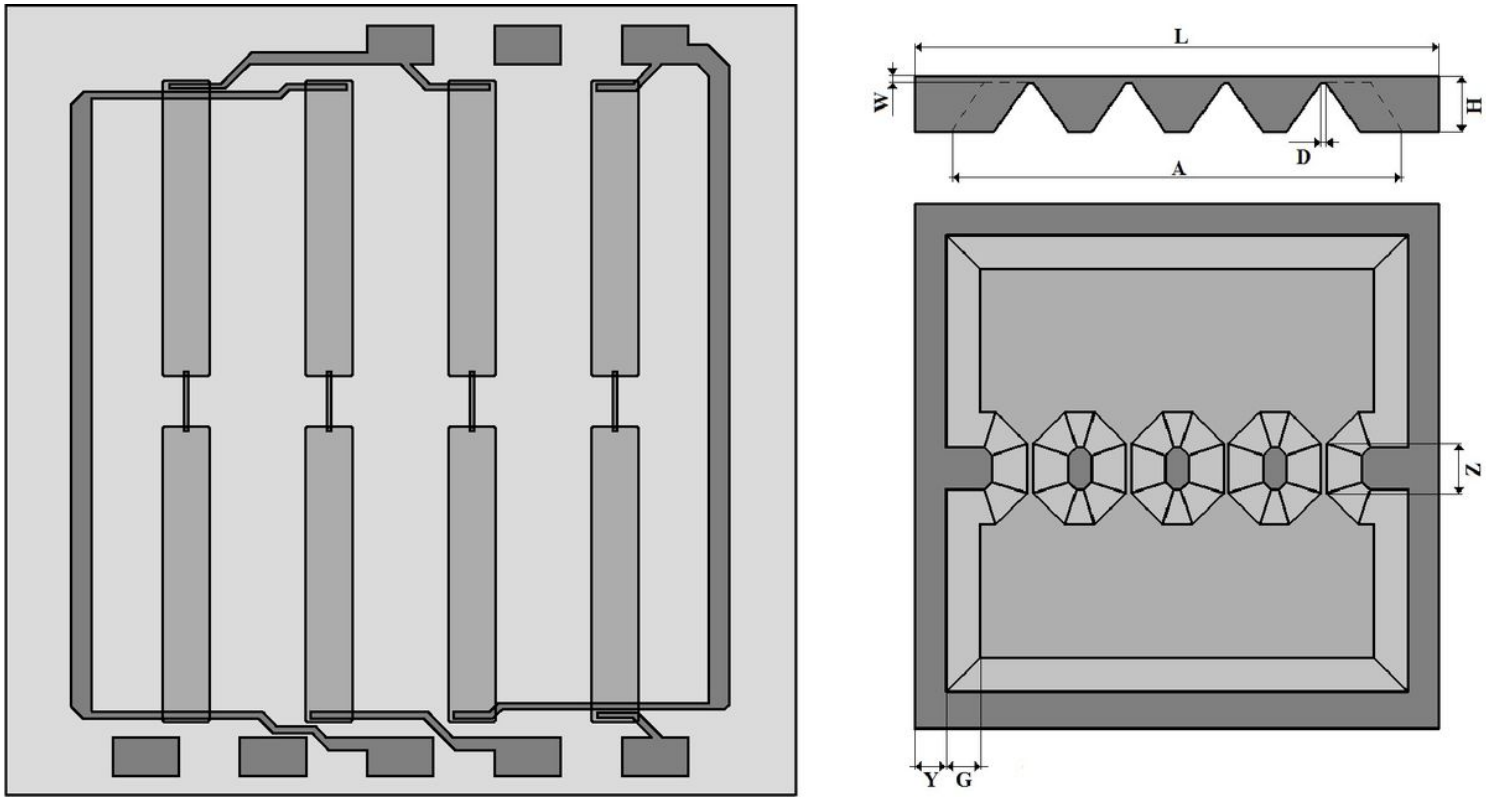

Figure 1

Fig. 1. Schematic representation of an ultrahigh sensitivity pressure sensor chip.

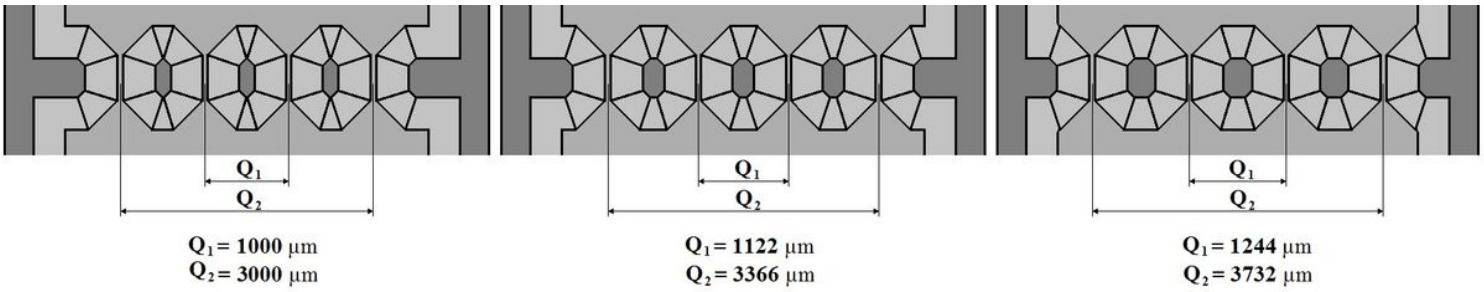

Figure 2

Fig. 2. Options of variation of RI width and, consequently, PR location on the membrane.

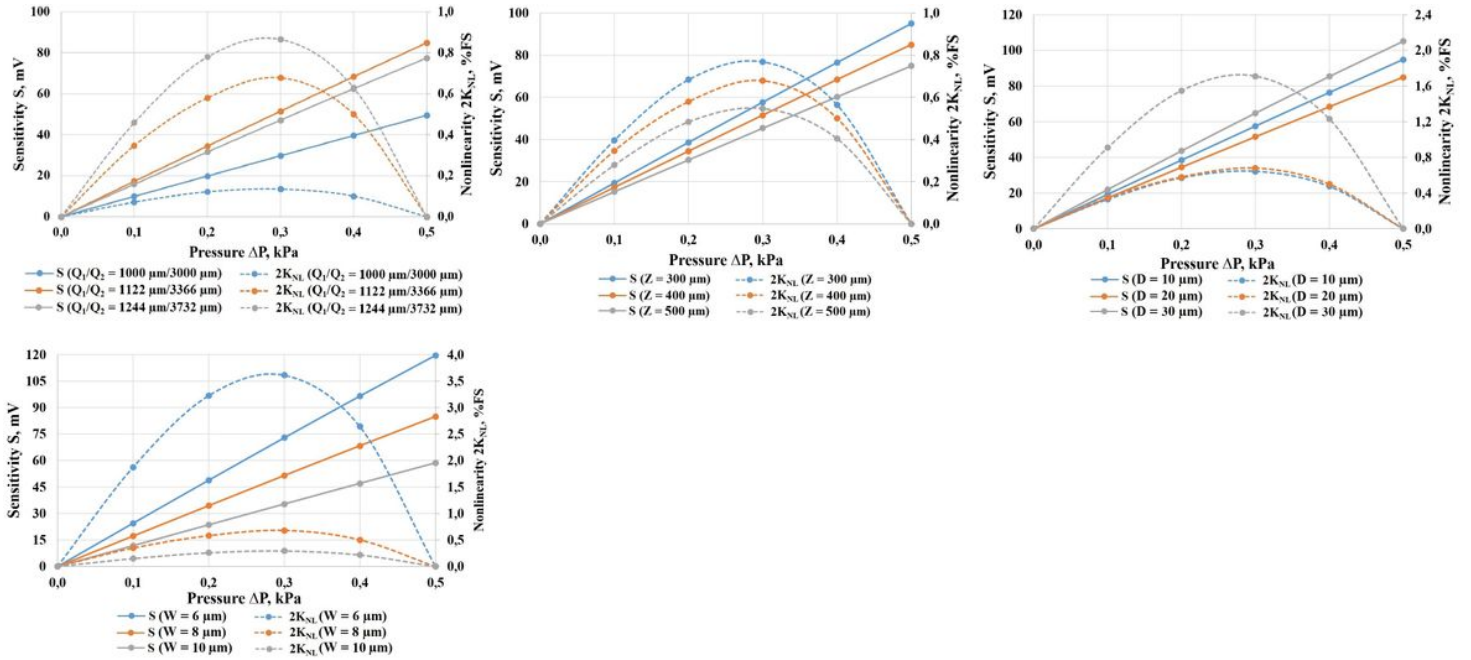

Figure 3

Sensitivity (solid line) and nonlinearity (dot line) dependences on the pressure at variation of: (a) RI width Q1/Q2, (b) RI edge length Z, (c) width of a gap between RIs D, (d) membrane thickness W.

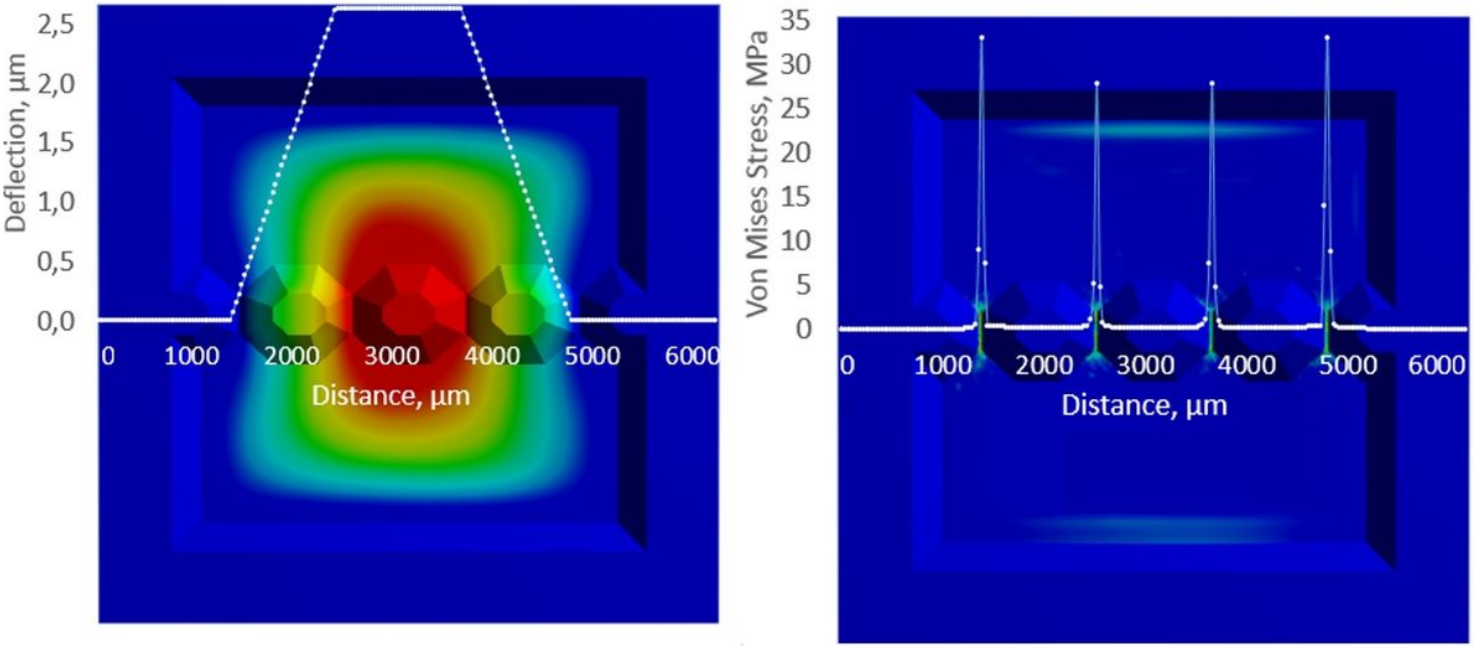

Figure 4

Maps of MS distribution (a) and membrane deflection (b) for the membrane geometry at 0.5 кPa.

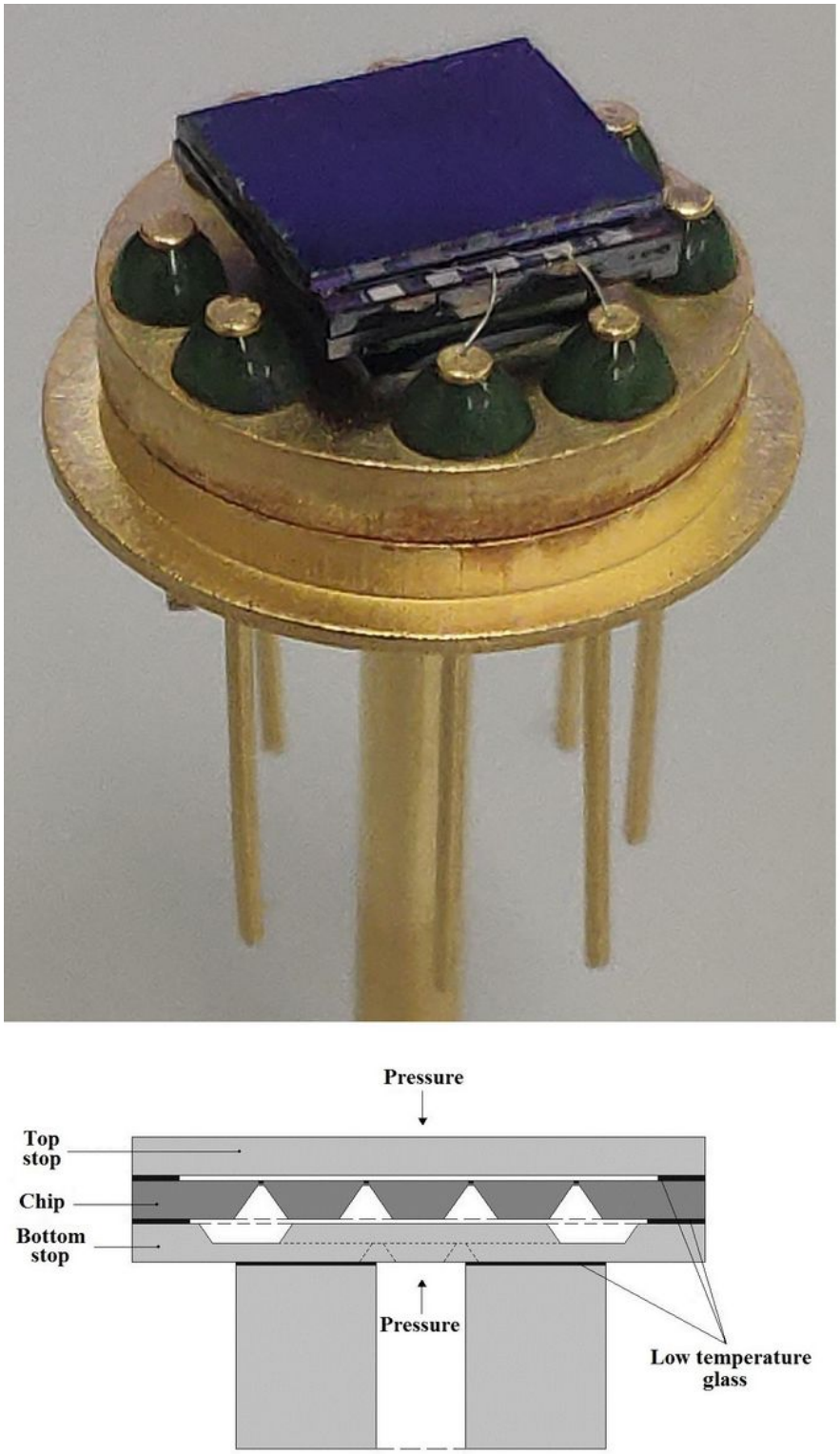

Figure 5

Assembly design: (a) schematic connection of a chip, stops and a base; (b) a pressure sensor assembly in the package.

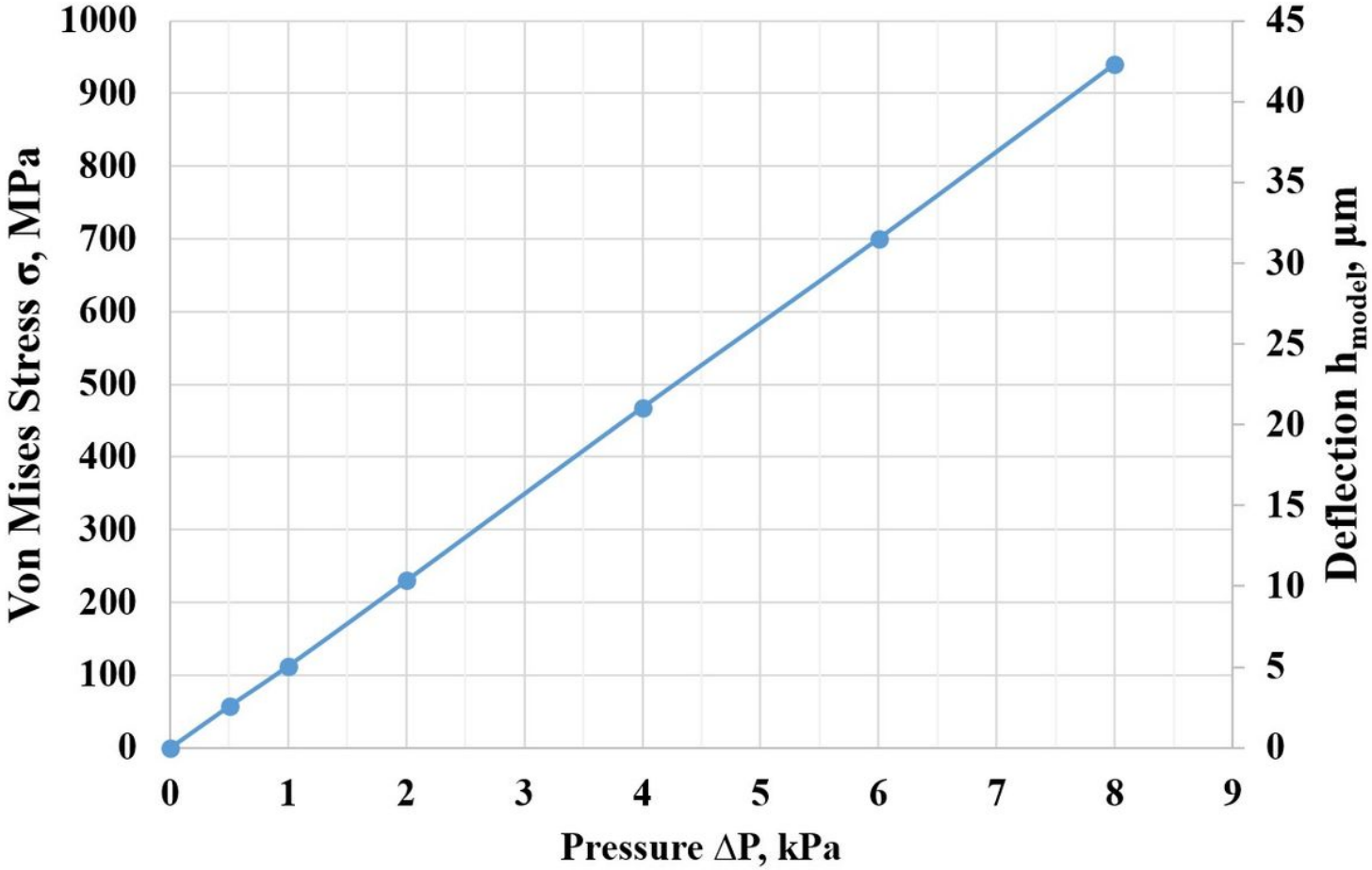

Figure 6

Fig. 6. Simulated dependence of end PR MS and the membrane middle deflection on the pressure (up to 8 κPa) for an ultrahigh sensitivity pressure sensor.

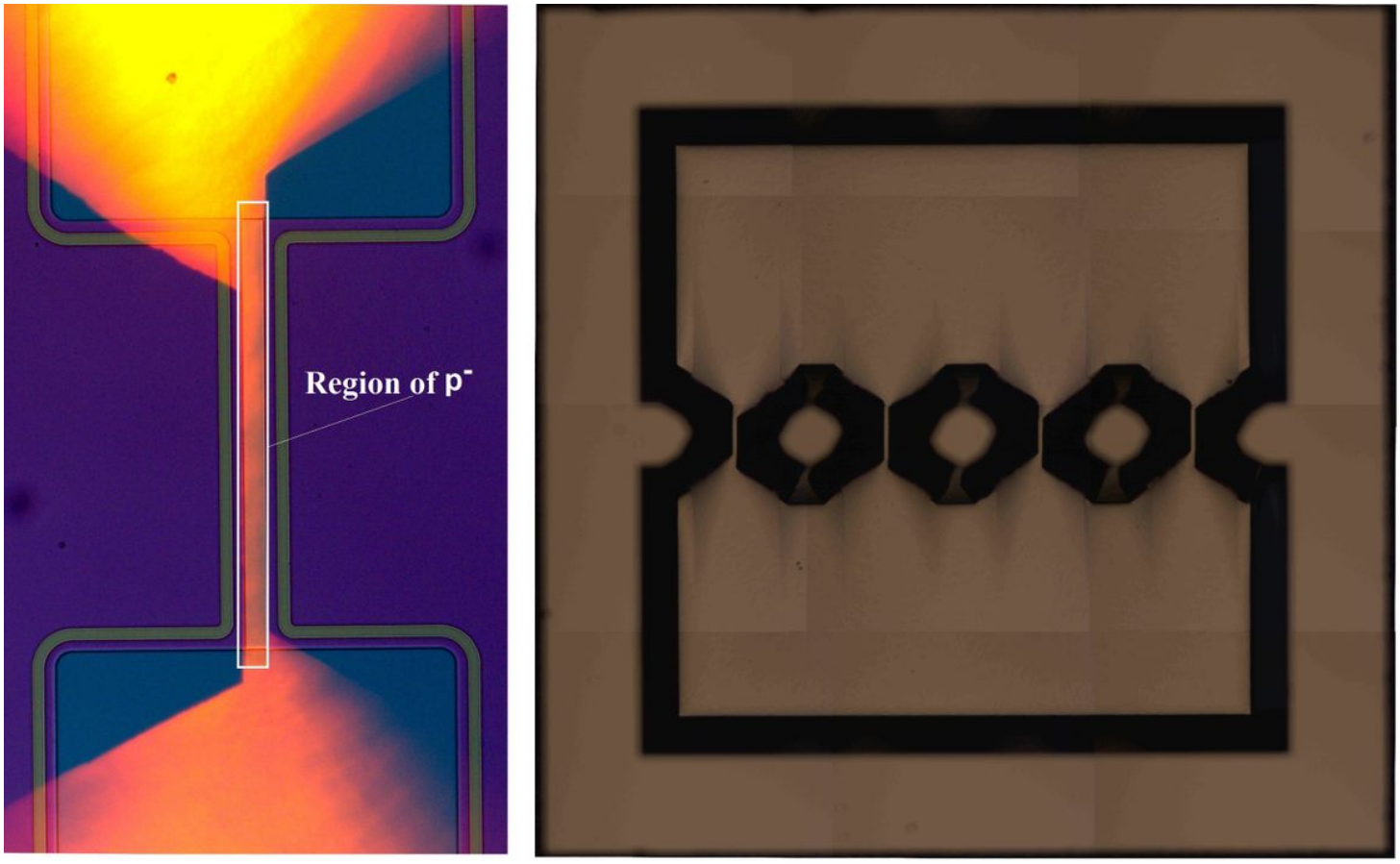

Figure 7

Membrane of experimental samples: (a) general view; (b) layout of PR p- -regions relative to RI structure.

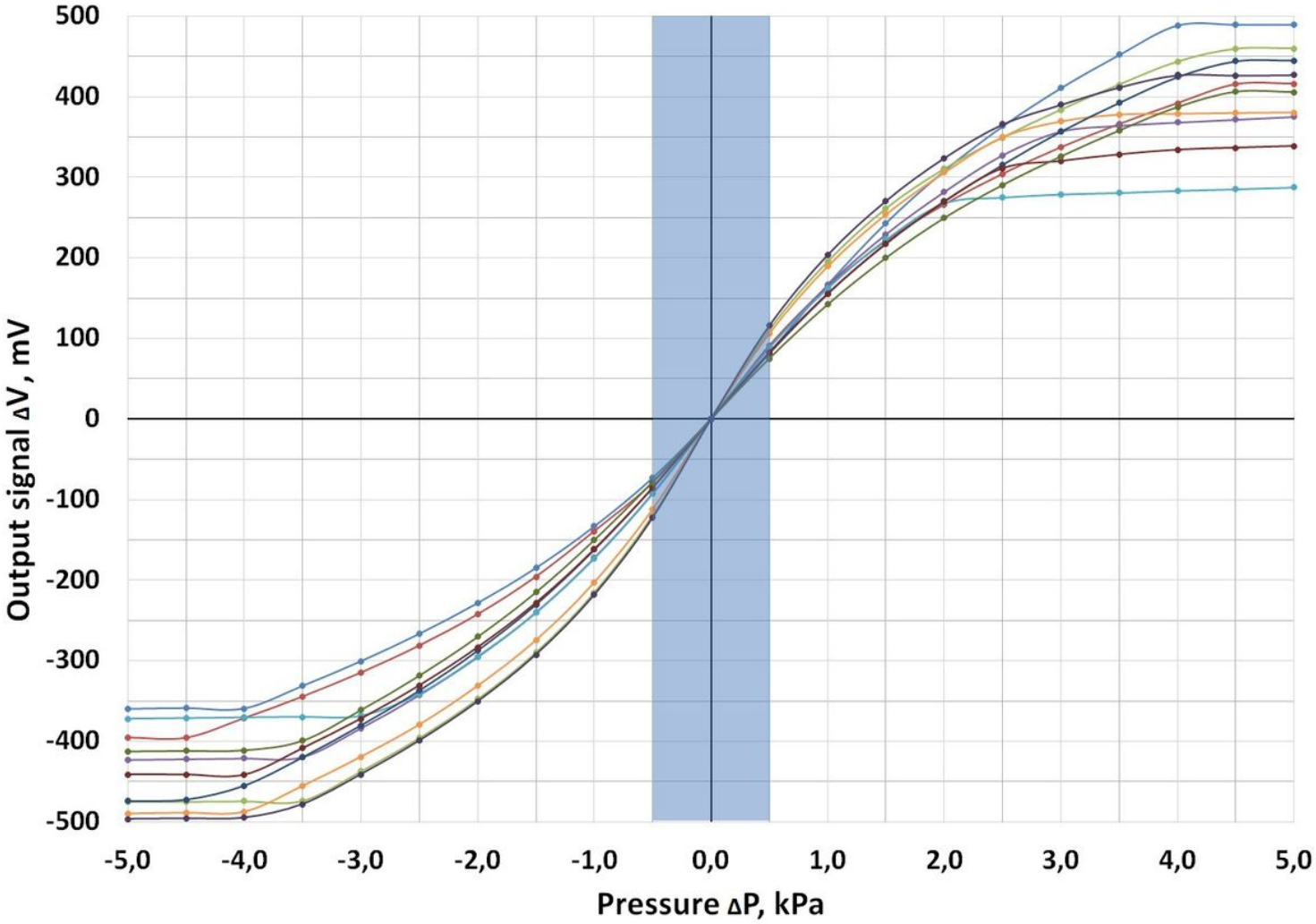

Figure 8

Fig. 8. Output signal dependencies on the pressure for several typical samples of an ultrahigh sensitivity pressure sensor.